JOURNAL OF MATERIALS SCIENCE 32 (1997) 4957–4965

Synthesis and growth mechanism of ThO_2–W–Mo alloy nanocomposite powder

X. DEVAUX, A. THOMY
Laboratoire de Métallurgie Physique & Science des Matériaux, URA CNRS 155 Ecole des Mines, 54042 Nancy Cedex, France

J. GHANBAJA
Service Commun de Microscopie Electronique, Université Henry Poincaré BP 239, F54506 Vandoeuvre les Nancy, France

Nanocomposite ultrafine powders of thorium oxide and tungsten molybdenum alloy were prepared by arcing between a pure molybdenum cathode and a thoriated tungsten anode under an argon–hydrogen atmosphere. The microstructure, morphology and chemical analyses of the ultrafine powders were examined by X-ray diffraction, transmission electron microscopy and associated techniques. The powders are composed of thorium oxide single-crystalline nano-grains decorated by tungsten molybdenum alloy particles which are crystallized in a metastable A15 structure. Two morphologies were observed: octahedra and needle-like particles. Every octahedral particle bigger than 15 nm had on each corner a metallic grain generally less than 8 nm in size. The needles had a length below 600 nm and their width to length ratio ranged from 1/3–1/15. They all presented on one of their ends a metallic particle which was comparable in size to the needle width. Other smaller particles (< 10 nm) may be encountered along the edges. The metallic particles were found to be epitaxial on the thorium oxide grains according to the relation: $(1\,0\,0)\,[0\,1\,1]_{ThO_2} \| (1\,0\,0)\,[0\,1\,1]_{A15}$. The extensive study of the microstructural and morphological properties of the powders leads us to suggest a growth mechanism of the nanocomposite particles.

1. Introduction

The study of nanostructured materials has attracted much attention in a variety of different fields. For instance, ceramic matrix nanocomposites are the subject of intensive work [1–5] intended, in particular, to improve the mechanical properties of ceramics. Enhancement of these properties by nanometric stiffening grains has been observed both in ceramic–ceramic [3] and in ceramic–metal systems [6–8].

Sintering or hot pressing of nanocomposite powders is an interesting method for the production of massive ceramic–metal nanocomposites. This process allows both the preparation of a closed mixture of phases and better control of the size and localization of the reinforcement nanoparticles [9, 10]. The use of nanocomposite ultrafine powders is a promising option to produce sintered massive nanocomposites [10].

The usual processes applied to the preparation of nanocomposite ultrafine particles are based on evaporation followed by condensation. A chemical synthesis in the vapour phase may be performed before the condensation. For example, Millers and Kuzjukevics [11] prepared Cr_2N–AlN and TiN–AlN nanocomposite powders in a plasmo-chemical process. In the same way, TiN–Me powders (Me = Fe, Co, Ni) have been synthesized in an arc furnace by coevaporation of metallic targets under a nitriding atmosphere [12, 13]. Complex growth mechanisms of the nanocomposite ultrafine powders lead to particular morphologies. One phase may be encapsulated in a second one (i.e. with the AlN–TiN composites [11]), or may be responsible for the growth of epitaxial whiskers (i.e. for AlN–Cr_2N [11] or for Me–carbon nanotubes [14]).

In this paper, we report a method for the production of ultrafine nanocomposite powders by evaporation of a composite target in an unreactive plasma arc in the case of the ThO_2–W–Mo alloys system. The extensive study of the microstructural and morphological properties of the powders will allow us to suggest a growth mechanism for the nanocomposite particles.

2. Experimental procedure

2.1. Specimen preparation

Fig. 1 shows a schematic illustration of the equipment used for producing ultrafine nanocomposite powders. It consists of an ultrafine powder generator, a powder collector and a gas circulator. ThO_2–W–Mo nanocomposite powders were prepared by evaporation and

0022–2461

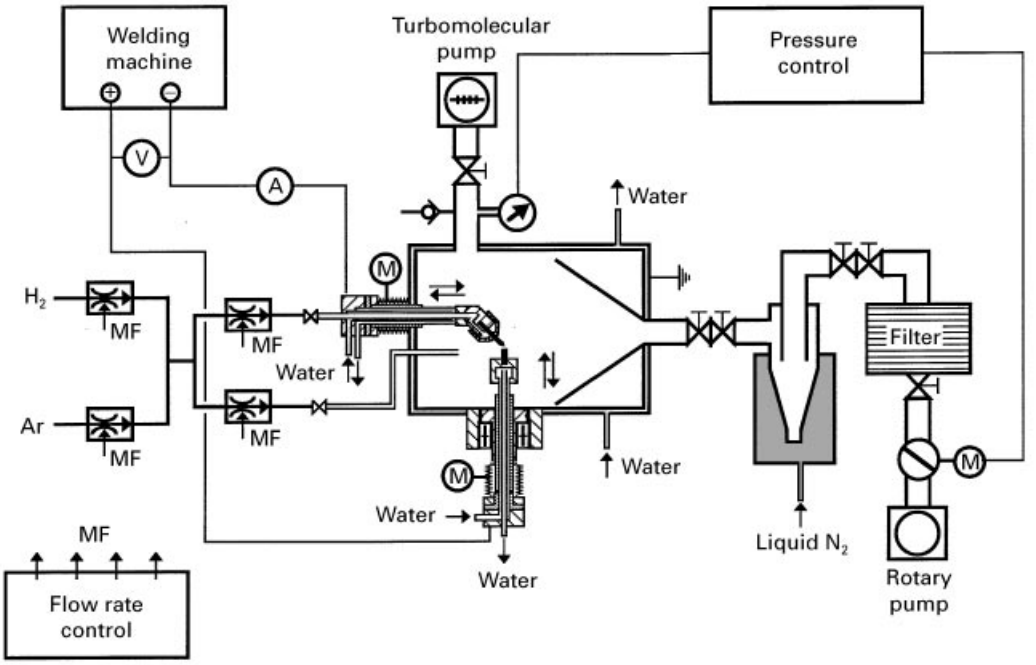

Figure 1 Schematic drawing of the pulverization apparatus. The cone in the pulverization chamber can be replaced by a water-cooled cylindrical condenser. A, ammeter; V, voltmeter; M, motor.

condensation of vapours obtained by heating pure molybdenum (99.95%) and thoriated tungsten (2 wt % ThO_2) rods of 4 mm diameter by a direct current arc discharge. The molybdenum rod was fixed in a water-cooled copper cathode and the thoriated tungsten electrode was kept in a water-cooled copper anode holder.

The arc was generated by a tungsten inert gas (TIG) welding machine. The smoke resulting from the condensation of vapours produced in the arc was carried out by a gas flow through a cryogenic heat exchanger, and was captured on a polytetrafluoroethylene (PTFE) membrane filter with a 0.2 μm porosity. The gas flow rates were managed by mass-flow controllers (MF) and were supported by a rotary pump located down stream of the filter. The pressure of the arc furnace was regulated by a butterfly valve mounted between the filter and the rotary pump. Before processing, the pulverization chamber and the filtration unit were evacuated down to about 5×10^{-4} Pa with a turbomolecular pump and then back-filled with the pulverization gases at the operating pressure. Powders trapped on the membrane filter were collected and preserved in a glove box under a high-purity argon atmosphere (H_2O and $O_2 < 1$ p.p.m.).

The pulverization experiments were fulfilled under 50% hydrogen – 50% argon mixture gas for a pressure of 2×10^4 Pa. The total gas flow rate was held constant at 10 l min^{-1}. The arc intensity and tension were maintained respectively, at 80 or 150 A and at 18 V for 1 h.

2.2. Characterization

The phase identification of the composite powders was determined by X-ray diffraction (XRD) on powders coated with collodion. About 100 mg powder were mixed with a solution of collodion (2 wt %) in isopentyl acetate and then deposited on a glass sample holder to avoid metal particle oxidation. After the evaporation of isopentyl acetate the powder was coated with a collodion film and could be handle in air without risk of oxidation. XRD analyses were performed on a Siemens D500 diffractometer using the Co$K_{\alpha 1}$ radiation ($\lambda = 0.1789$ nm).

The powder microstructures were studied in Jeol 200CX and Philips CM20 transmission electron microscopes (TEM) at 200 kV operating tension. Energy dispersive X-ray (EDX) semi-quantitative analyses were performed in the CM20 TEM with an EDAX spectrometer. As for XRD investigations, the powders were dispersed in a collodion solution under ultrasonic stirring, then one drop of the obtained stable suspension was deposited on the surface of distilled and ultra-filtered water. The resulting film was deposited on a 200 mesh copper grid and strengthened with a thin layer of carbon obtained by evaporation [15]. Copper peaks were systematically observed on the EDX analyses spectra. These peaks result from an interfering signal coming from the copper grid sample holder.

3. Results and discussion

3.1. Phase identification

By setting up the electric arc, the top of the thoriated tungsten electrode melted almost instantaneously and thin smoke emanated from the plasma zone. During processing, some small incandescent droplets spattered from the melted metallic drop of the anode top. After 1 h pulverization, the molybdenum cathode and the thoriated tungsten anode were slightly eroded. The pulverization yield reached 600 mg h^{-1} for 150 A arc and was less than 300 mg h^{-1} for 80 A arc. It was

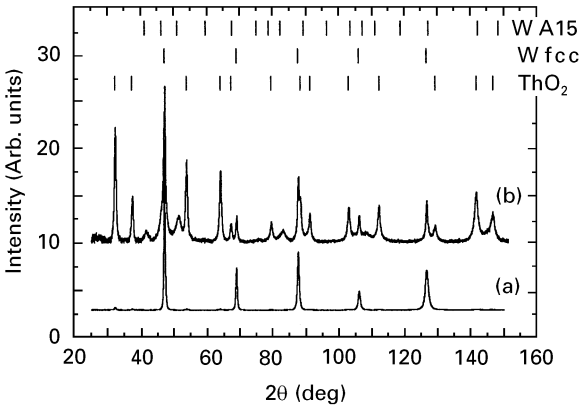

Figure 2 Typical example of XRD diagrams. (a) Ground thoriated tungsten electrode; (b) As-produced powder trapped on the filter.

noticed that 50 wt % of the smoke was trapped on the filter. The as-prepared powders were highly agglomerated, black in colour and contained some small solidified droplets visible to the naked eye.

XRD patterns of ground as-received tungsten electrode and powder trapped on the PTFE membrane are presented in Fig. 2. The theoretical positions of the diffraction peaks of ThO_2, body-centred cubic (b c c) tungsten and W-A15 phases are marked on the same figure. On the electrode diagram, only b c c tungsten and cubic thorium oxide phases are detectable (diagram a). The thorium oxide phase has a weak signal because of its low abundance in the electrode (2 wt %). Three phases are visible on the powder pattern (diagram b): the same phases as in the electrode, and a third one which was identified as an A15 cubic phase. The peak intensity of the thorium oxide phase shows a high ThO_2 content of the powders. The lattice parameters measured on the XRD diagram of the b c c tungsten phase and thorium oxide are the same as the theoretical lattice parameters, corresponding to pure b c c tungsten and stoichiometric ThO_2 compound. The A15 structure was previously found on ultrafine metallic particles of the VI_A metals group when these were produced by thermal [16, 17] or electron-beam evaporation [18] or sputtering [19] under a low pressure of a pure rare gas (helium or argon). The values of the lattice parameters of W–A15 and Mo–A15 structures deduced from the electron diffraction patterns were estimated, respectively, as 0.509 ± 0.003 nm and 0.501 ± 0.003 nm by Saito *et al.* [17]. On our XRD diagrams, we observed an A15 structure with a lattice parameter of 0.506 ± 0.002 nm. By assuming that the W–A15 and Mo–A15 phases are completely soluble and that the lattice parameters of the alloys conform to the Vegard rule, about 30 at % Mo could be dissolved in W–A15 phase.

3.2. Microstructural characterization

Electron microscopy investigations showed three types of particle in the powder prepared in the 150 A arc. Some particles have a spherical shape and their size ranges from some micrometres to a fraction of a millimetre. EDX semi-quantitative analyses show the grains are constituted of tungsten. They find their origin in the spattered droplets seen during the pulverization. We noted from electron diffraction that these grains have a b c c structure. The other particles have a submicrometric size and have a composite appearance. Two morphologies are observable on transmission electron micrographs: needle-shaped nanocomposite particles (Fig. 3a) and octahedral shaped nanocomposite particles (Fig. 3b).

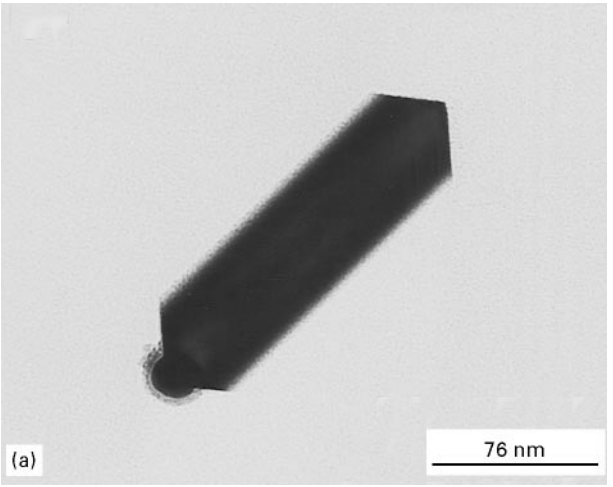

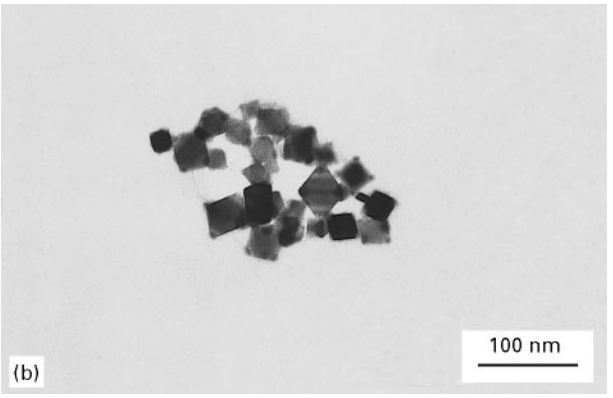

Figure 3 Bright-field transmission electron micrographs of ThO_2–W–Mo nanocomposite powder. (a) An isolated needle-like particle; (b) a group of octahedral particles.

3.2.1. Needle-like grain investigations

Every needle examined in our samples had the same general morphology. They were faceted and their length ranged from 25–600 nm. Their width to length ratio varied from 1/3 for the smallest needles to 1/15 for the longest. All of them had, on one of their ends, a faceted or a spherical particle with a size comparable to the needle width. Other much smaller particles ($2 \text{ nm} < d < 10 \text{ nm}$) may decorate the edges along the length of the needle and on the end corners opposite to the largest metallic particle (Fig. 4a).

EDX analyses showed the needle body is only constituted of thorium oxide (Fig. 4f). The end and the edge particles contain tungsten and molybdenum (Fig. 4g). The ratio of the tungsten to molybdenum atomic contents ranges from 1/5–1/3. Statistical

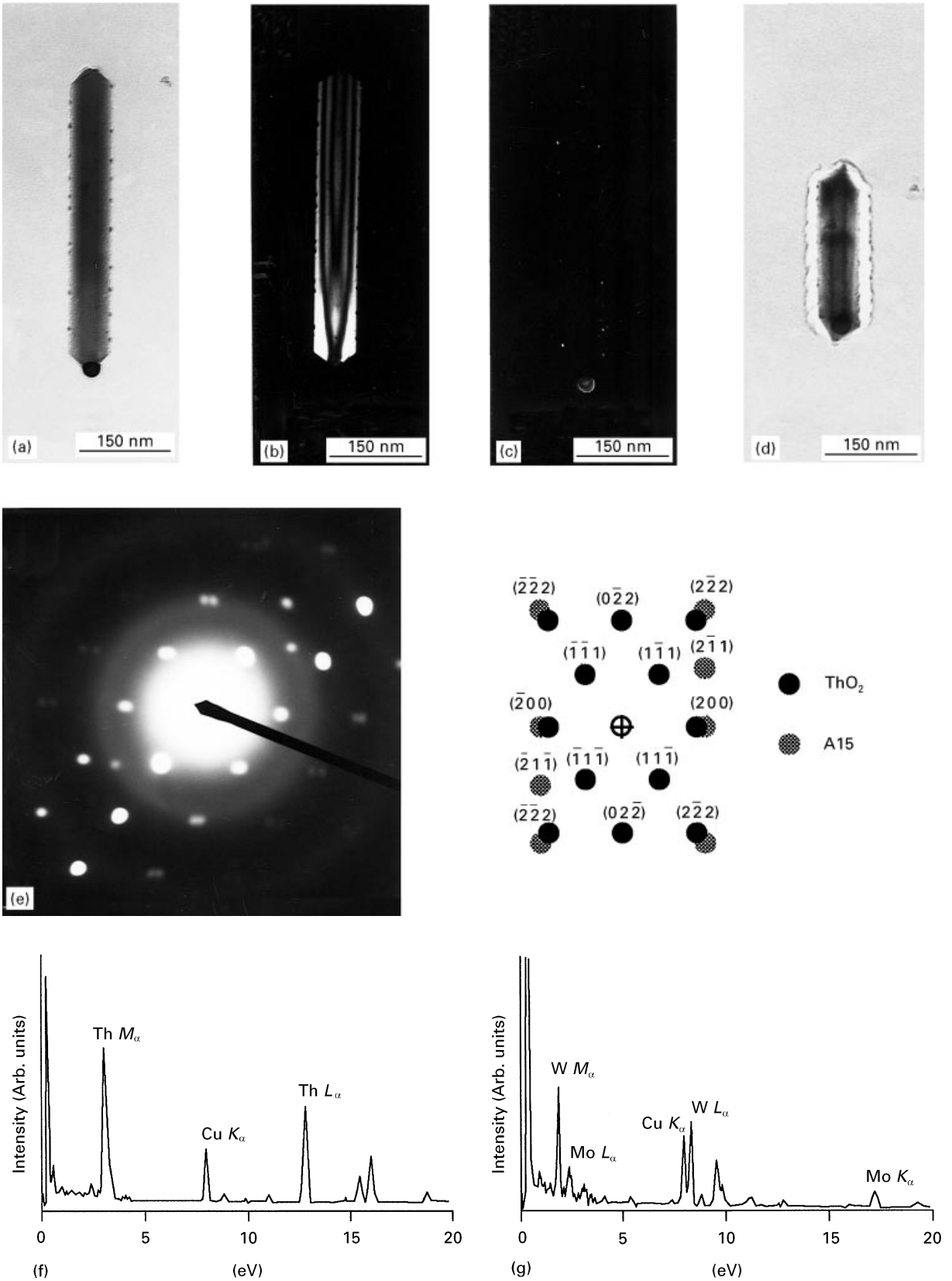

Figure 4 TEM analysis of a needle. (a) Bright-field of a needle ($[0\,1\,1]_{ThO_2}$ orientation), (b) $\bar{1}\,1\,\bar{1}_{ThO_2}$ dark-field, (c) $\bar{2}\,1\,\bar{1}_{A15}$ dark-field, (d) location of the end metal particle, (e) electron diffraction pattern of the needle with the electron-beam parallel to the direction $[0\,1\,1]_{ThO_2}$, (f) EDX analysis of the needle body, (g) EDX analysis of the end metallic particle.

semi-quantitative measurements on about 100 particles show the end-alloyed tungsten–molybdenum grains contains 28 at % Mo. This chemical analysis is in agreement with the lattice parameter deduced from XRD diagrams.

Electron diffraction patterns show the thorium oxide needles are single crystalline (Fig. 4e). Fig. 4b shows a dark-field electron micrograph obtained with a $\bar{1}\,1\,\bar{1}_{ThO_2}$ diffraction spot. The long axis of the needle was indexed as a $[0\,1\,\bar{1}]_{ThO_2}$ type axis. For the metallic

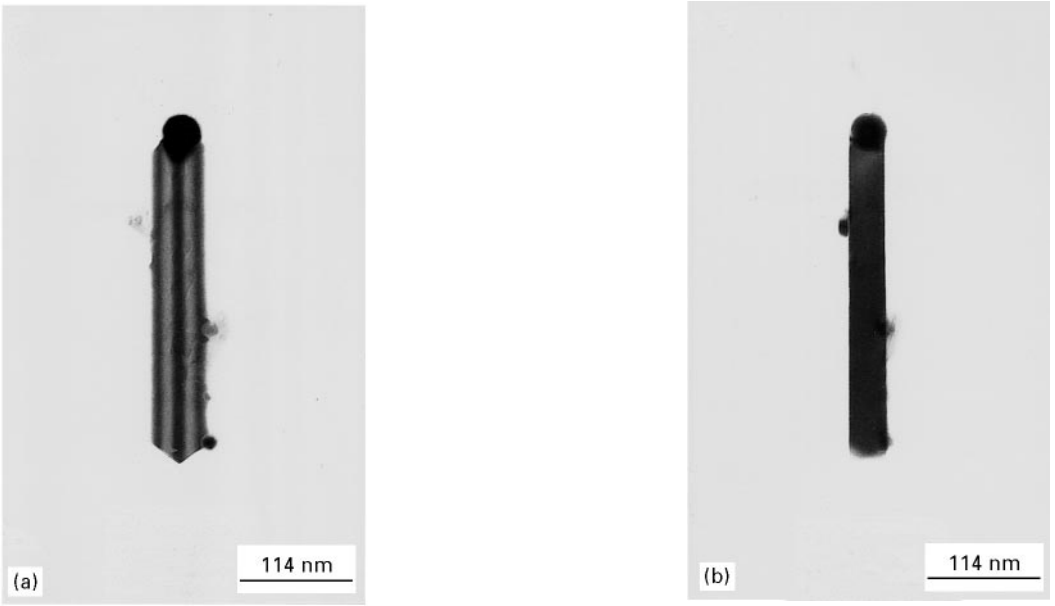

Figure 5 Identification of the needle faces: (a) electron beam oriented along the $[0\,1\,1]_{ThO_2}$ zone axis, identification of the end faces; (b) electron beam oriented along the $[2\,1\,\bar{1}]_{ThO_2}$ direction, identification of faces along the needle.

phase, only an A15 structure is detectable on the electron diffraction pattern. As shown in the dark-field micrograph realized with a $\bar{2}\,1\,\bar{1}_{A15}$ diffraction spot, all the metallic particles have the same orientation (Fig. 4c). The epitaxial relationship noticed between the thorium needle and the tungsten alloy particles is described by $(1\,0\,0)[0\,1\,1]_{ThO_2} \| (1\,0\,0)[0\,1\,1]_{A15}$. By tilting the nanocomposite particle presented on Fig. 4a by 50° around the $[1\,3\,\bar{1}]_{ThO_2}$ direction, we notice (Fig. 4d) that the large W–Mo alloy grain is epitaxial to an edge of the thorium oxide needle, close to a corner. Tilting by 55° of a needle facing a $[0\,1\,1]_{ThO_2}$ zone axis (Fig. 5a) around the $[0\,1\,\bar{1}]_{ThO_2}$ direction, reveals that the needle is lying flat on one of their faces, the new zone axis parallel to the electron beam being $[2\,1\,\bar{1}]_{ThO_2}$ (Fig. 5b). The study of the electron diffraction patterns and the shapes of the needle appearing on the two transmission electron micrographs, lead us to conclude that the needles are surrounded by faces of $\{1\,1\,1\}$ type planes. They are like an octahedron drawn to a $[0\,1\,1]_{ThO_2}$ type direction.

3.2.2. Octahedral nanocomposite grain analyses

The octahedral particles have a size ranging from 15–70 nm. By tilting the octahedra we saw that each corner of every particle is coated with a small grain which ranges in size from 2–8 nm. On a given octahedron, each grain has the same size. We never found any particles on the octahedral faces or edges. Fig. 6a shows an octahedral particle on one of its edges and Fig. 6b shows the same particle on one of its corners. The latter micrograph reveals that a particle is present on each corner of the octahedron.

EDX analyses showed that the body of the octahedral nanocomposite powders is only constituted of thorium oxide, as was detected on the needles (Fig. 6d). The corners coated with particles contain only tungsten and molybdenum (Fig. 6e). The same tungsten to molybdenum ratio was found as previously, for the needle case. The small oxidation layer seen around the metallic particles on the bright-field micrographs (Fig. 6a and b) probably appears during handling of the powders. Electron diffraction pattern analyses (Fig. 6c) lead to the same crystallographic measurement as on the needles, like nanocomposite grains: metallic particles have a A15 structure; metallic particles have the same crystallographic orientation and are epitaxial according to the relation: $(1\,0\,0)[0\,1\,1]_{ThO_2} \| (1\,0\,0)[0\,1\,1]_{A15}$; the thorium oxide particles of octahedral habit are surrounded by $\{1\,1\,1\}$ type facets.

Some nanocomposite powders were exposed to air for 1 month. Surprisingly, we observed by transmission electron microscopy that most of the oxidized metallic grains came away of the needles and the octahedra. Fig. 7 shows the result of the oxidation on nanocomposite octahedra. The corners of these octahedral particles appear truncated and pitted. This observation indicates that the metallic particles were partially embedded in the thorium oxide matrix before oxidation. This result provides some information on the growth process of the nanocomposite ultrafine powders, as will be revealed in the next section.

3.3. Nanocomposite particle growth

To investigate the growth mechanism of the nanocomposite grains, we tried to reduce the powder size. The size and the number of nucleated grains can be significantly affected in plasma processes by controlling the cooling rate at the nucleation zone and the concentration of the condensable vapour [20, 21]. Actually, to decrease the particle growth, the cooling rate has to be

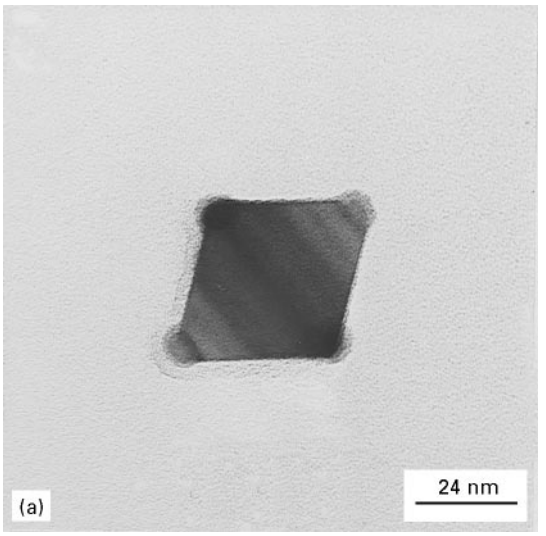

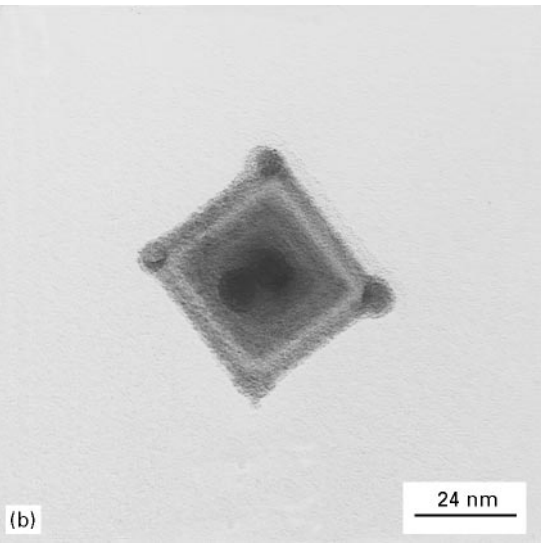

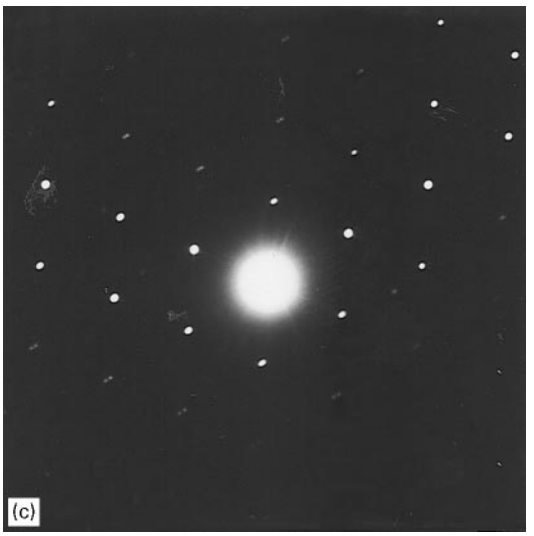

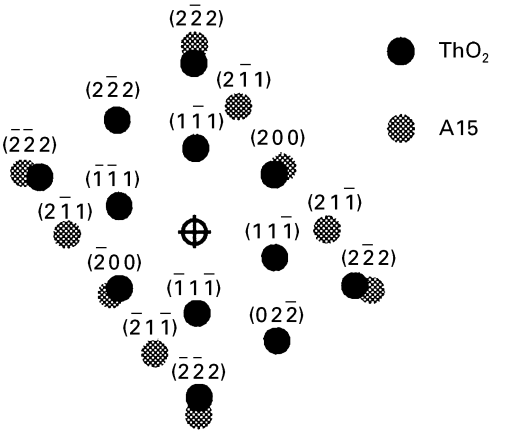

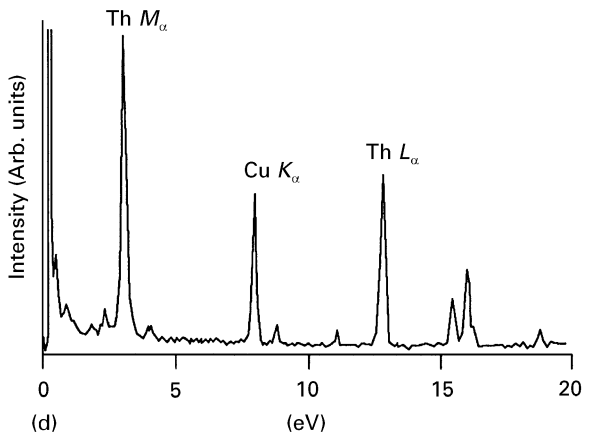

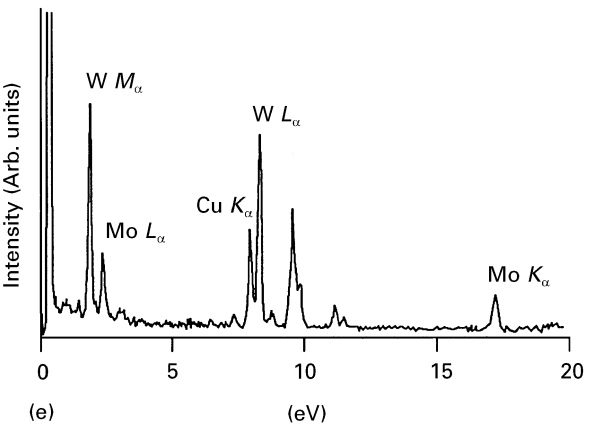

Figure 6 TEM analysis of an octahedral particle. (a) Bright-field of an isolated particle laid on one of its edges ($[0\,1\,1]_{ThO_2}$ orientation); (b) bright-field of the same particle on one of its corners; (c) electron diffraction pattern of the nanocomposite octahedron, electron beam parallel to the direction $[0\,1\,1]_{ThO_2}$; (d) EDX analysis of the body of the octahedral particle; (e) EDX analysis of a particle coated on a corner.

increased and the condensable species have to be decreased. The increase in the cooling rate was obtained by increasing the gas flow up to 20 l min^{-1} and by replacing the cone of the pulverization chamber by a water-cooled tubular condenser (Fig. 1) which allows the powder to be sampled close to the anode. The limitation of the evaporation yield was reached by decreasing the arc intensity down to 80 A. To eliminate the molybdenum influence on nucleation and growth, the powders were prepared by arcing between two thoriated tungsten electrodes.

The change in the operating parameters significantly reduced the mean size of the particles. Nevertheless, the same powder morphologies and

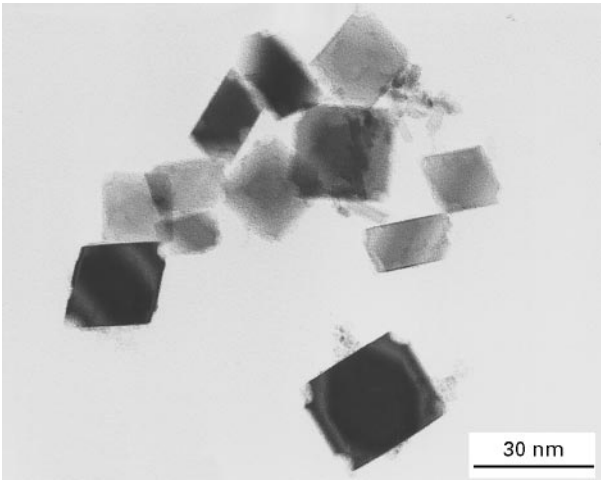

Figure 7 Bright-field transmission electron micrograph of an oxidized octahedral particle.

micro-structures as those previously described were systematically found on the new samples. Octahedral and needle-like particles were observed. However, the length of most of the needles did not exceed 30 nm and many octahedral grains had sides < 10 nm long.

Even on the smallest needles (< 25 nm long and 10 nm wide) a metallic particle was systematically observed on one of their ends. The diameter of this metallic particle was of the same order of magnitude as the needle width (Fig. 8a). Only the bigger needles present some metallic grains along their edges and on their corners (Fig. 8b).

While all the bigger thorium oxide octahedra have metallic grains epitaxial to their corners (Fig. 8d), no metallic particles were observed on octahedral grains smaller than 10 nm (Fig. 8c), either because they were too small to be seen, or more probably because they did not exist.

According to the TEM characterization, the nanocomposite particles are presumed to be formed through the processes shown in Fig. 9. The vapour emitted from the electrodes (stage 1) condenses either as thorium oxide or tungsten alloy nuclei (stage 2). After growth from the vapour phase, these single-crystalline grains serve as a site of heterogeneous nucleation for the second phase.

In the octahedron case, the oxide particles increase to a size larger than 10 nm (stage 3a) before serving as sites for the heterogeneous nucleation of the metallic phase (stage 4a). As the metal particles are partially embedded in the corners of

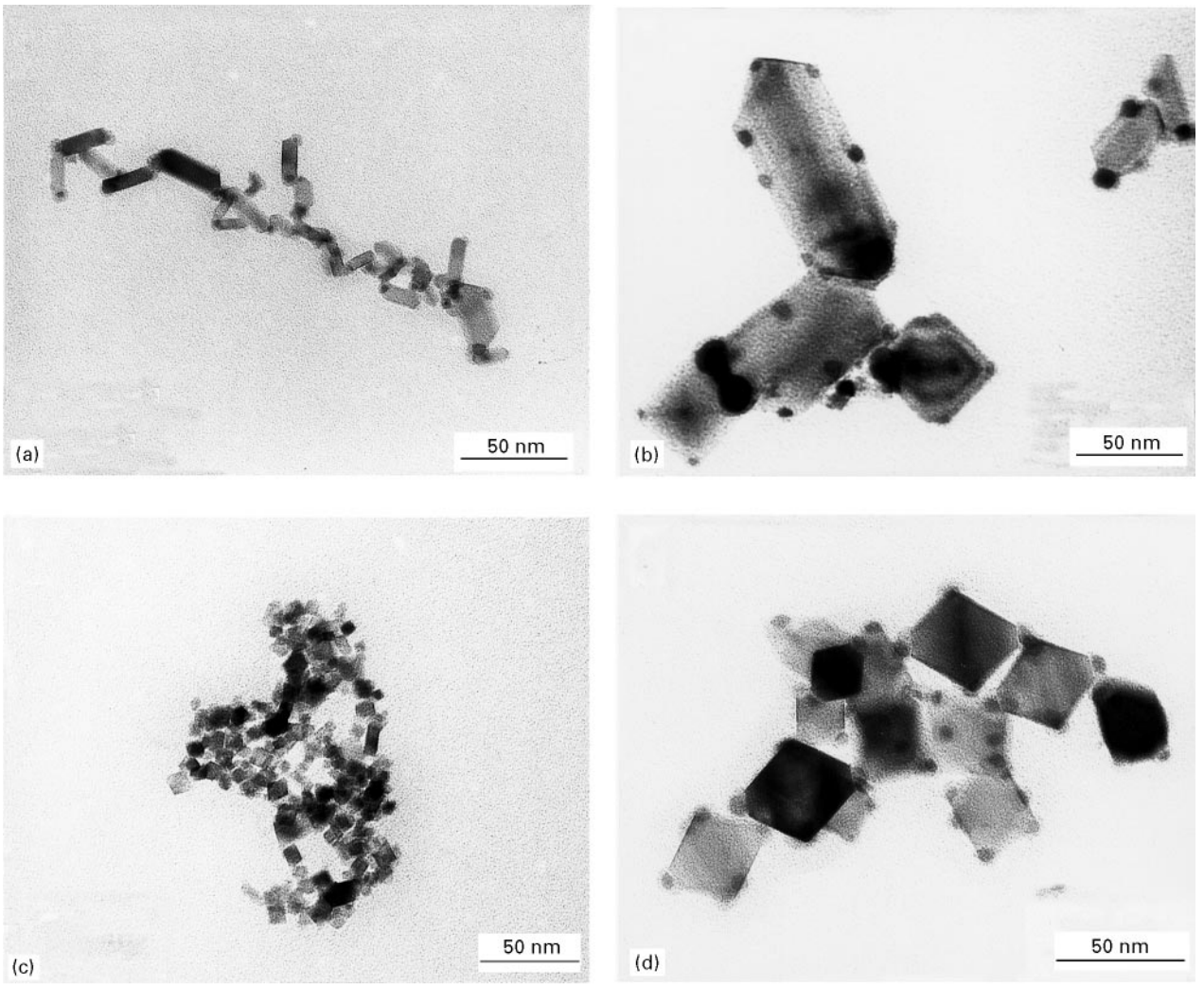

Figure 8 Bright-field transmission electron micrographs of ThO_2–W nanocomposite powders. (a) The smallest needles, (b) larger needles, (c) Octahedra smaller than 10 nm without coated metallic particles; (d) Octahedra larger than 10 nm with coated metallic grains.

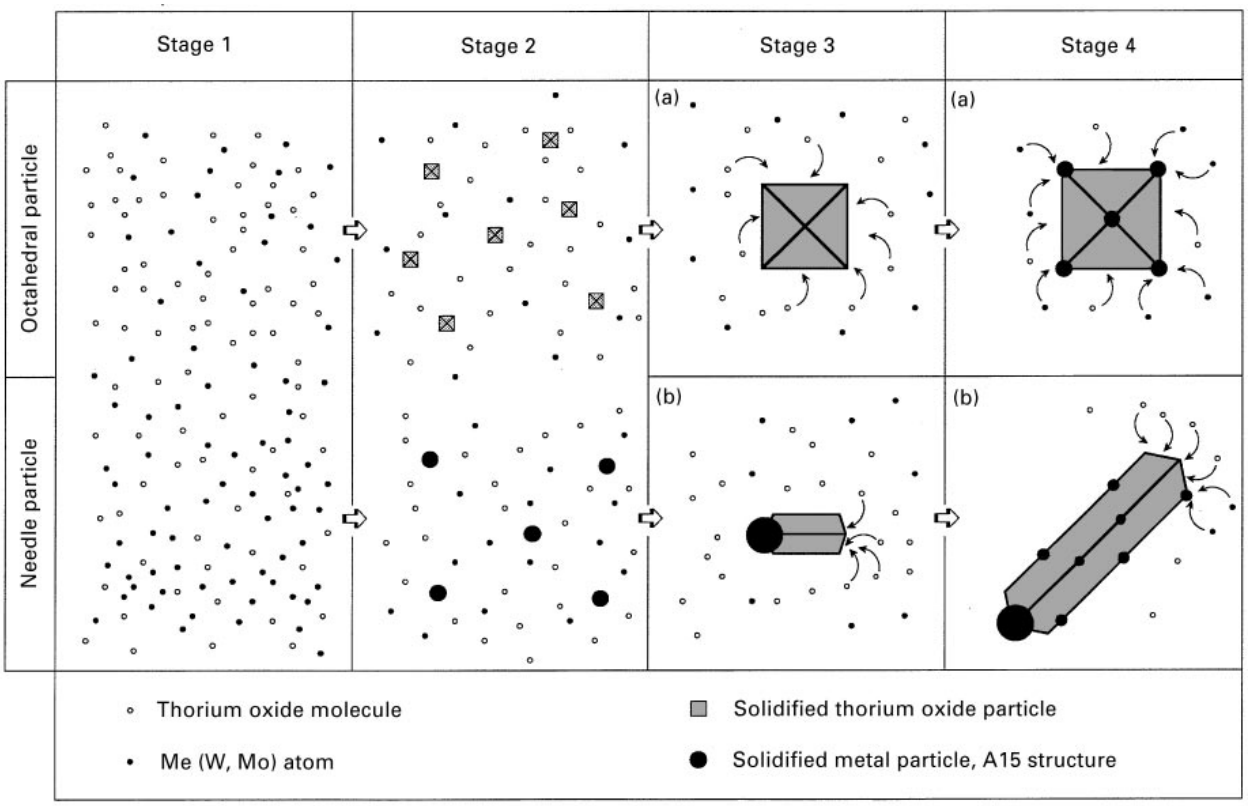

Figure 9 Schematic illustration of the proposed mechanism of nucleation and growth of the nanocomposite grains. Stage 1, vapour production; Stage 2, homogeneous nucleation; Stage 3a, growth of the thorium oxide octahedron; Stage 3b, heterogeneous nucleation of thorium oxide on a metallic particle; Stage 4a, heterogeneous nucleation of metal on the corners of the octahedral grain; Stage 4b, heterogeneous nucleation of metal on the needle corners and growth of the thorium oxide needle.

the octahedra, the thorium grains cease to grow after the growth of the metallic particles. The systematic existence of metallic grains on all the corners of thorium oxide octahedra larger than 10 nm, tends to exclude these nanocomposite particles being formed by collision between metallic and oxide grains.

The needle growth is more complex. Because we observed that every needle less than 10 nm long systematically has a metallic particle with a size of the same order of magnitude as the needle width, it is highly probable that the needles were created by heterogeneous nucleation of the thorium oxide on metallic grains. The thorium oxide preferentially grows along a [0 1 1] direction (stage 3b). The existence of metallic particles on the needle edges can be explained by the heterogeneous nucleation of metal during the growth of the oxide particles. During oxide growth, metallic vapour may nucleate on the corners of the needle, as in the case for octahedra (stage 4b). After needle growth, metallic particles nucleated during needle development appear to be partially embedded in the needle edges.

4. Conclusion

Nanocomposite ultrafine powders of thorium oxide and tungsten molybdenum alloy were prepared in an arc furnace by arcing between a pure molybdenum cathode and a thoriated tungsten anode. The nanocomposite powders were composed of a single-crystalline body of pure thorium oxide decorated by metallic particles. XRD and electron microdiffraction investigations showed the metallic grains to have A15 structure. Metallic particles contain about 28 at % Mo. We should emphasize that this alloy was obtained for the first time with A15 structure. Two morphologies were observed on the nanocomposite powders: needles and octahedra. On each corner of the thorium oxide octahedron, a tungsten molybdenum alloy nanoparticle was partially embedded. The faces of the thorium oxide needles were identified as $\{1\,1\,1\}$ type planes. They present, on one of their ends, a large metal particle, and smaller ones may be seen along the edges and on the corners. Electron diffraction analyses showed the metallic particles to be epitaxial to the thorium grains according to the relation $(1\,0\,0)[0\,1\,1]_{ThO_2} \| (1\,0\,0)[0\,1\,1]_{A15}$. The microstructural study of powders prepared by arcing between two thoriated tungsten electrodes has allowed a growth mechanism of the powders to be proposed. This process is based on the simultaneous homogeneous nucleation of thorium oxide and metallic alloy, followed by the heterogeneous nucleation of a second phase on the first. The heterogeneous nucleation of thorium oxide on one tungsten alloy particle leads to the growth of a needle. The heterogeneous nucleation of tungsten alloy on one thorium oxide grain leads to an octahedral nanocomposite particle.

Acknowledgement

The authors thank Dr M. Brieu, Laboratoire de Chimie des Matériaux Inorganiques, Université Paul Sabatier, Toulouse, France, for useful discussions.

References

1. R. ROY, *Mater. Res. Soc. Symp. Proc.* **286** (1993) 241.
2. S. KOMARENI, *J. Mater. Chem.* **2** (1992) 1219.
3. K. NIIHARA, *Nippon Seram. Kyokai Gakuyutsu Ronbunshi* **99** (1991) 974.
4. X. DEVAUX, Ch. LAURENT and A. ROUSSET, *J. Alloys Compounds* **188** (1992) 179.
5. A. MARCHAND, X. DEVAUX, B. BARBARA, P. MOLLARD, M. BRIEU and A. ROUSSET, *J. Mater. Sci.* **28** (1993) 2217.
6. T. SEKINO, A. NAKAHIRA, M. NAWA and K. NIIHARA, *J. Jpn Soc. Powder Powder Metall.* **38** (1991) 326.
7. X. DEVAUX, Ch. LAURENT, M. BRIEU and A. ROUSSET, in "Composite Materials", edited by A.T. Di Benedeto, L. Nicolais and R. Watanabe (Elsevier Science, Amsterdam, 1992) p. 209.
8. M. NAWA, T. SEKINO and K. NIIHARA, *J. Mater. Sci.* **29** (1994) 3185.
9. X. DEVAUX, Ch. LAURENT and A. ROUSSET, *Nanostruct. Mater.* **2** (1993) 339.
10. T. KIZUKA, H. ICHINOSE and Y. ISHIDA, *J. Mater. Sci.* **29** (1994) 3107.
11. T. N. MILLERS and A. A. KUZJUKEVICS, *Prog. Crystal. Growth Charact.* **16** (1988) 367.
12. S. OHNO, *J. Jpn Weld. Soc.* **59** (1990) 115.
13. S. OHNO, K. HONMA, H. OKUYAMA and M. OZAWA, *J. Jpn. Inst. Metals* **53** (1989) 936.
14. Y. SAITO, T. YOSHIKAWA, M. OKUDA, N. FUJIMOTO, K. SUMIYAMA, K. SUZUKI, A. KASUYA and Y. NISHINA, *J. Phys. Chem. Solids* **54** (1993) 1849.
15. M. BRIEU, PhD Thesis, Université Toulouse III, France (1986).
16. K. KIMOTO and I. NISHIDA, *J. Phys. Soc. Jpn* **22** (1967) 744.
17. Y. SAITO, K. MIHAMA and R. UYEDA, *Jpn J. Appl. Phys.* **19** (1980) 1603.
18. S. IWAMA and K. HAYAKAWA, *Surf. Sci.* **156** (1985) 85.
19. S. YATSUYA, T. KAMAKURA, K. YAMAUCHI and K. MIHAMA, *Jpn. J. Appl. Phys.* **25** (1986) L42.
20. S. L. GIRSHICK, C. P. CHIU and P. H. McMURRY, *Plasma Chem. Plasma Process.* **8** (1988) 145.
21. M. H. TENG, J. J. HOST, J. H. HWANG, B. R. ELLIOTT, J. R. WEERTMAN, T. O. MASON, V. P. DRAVID and D. L. JOHNSON, *J. Mater. Res.* **10** (1995) 233.

Received 30 November 1995
and accepted 4 April 1997